Wood Kimberly, M. (Orcid ID: 0000-0002-1436-5137)
Klotzbach Philip (Orcid ID: 0000-0001-5372-6241)
Collins Jennifer, M (Orcid ID: 0000-0001-6780-8280)
Caron Louis-Philippe (Orcid ID: 0000-0001-5221-0147)
Truchelut Ryan, Eugene (Orcid ID: 0000-0002-7251-695X)

Factors affecting the 2019 Atlantic hurricane season and the role of the Indian Ocean Dipole

Kimberly M. Wood[1], Philip J. Klotzbach[2], Jennifer M. Collins[3], Louis-Philippe Caron[4], Ryan E. Truchelut[5], Carl J. Schreck[6]

[1]Department of Geosciences, Mississippi State University, Mississippi State, MS, USA

[2]Department of Atmospheric Science, Colorado State University, Fort Collins, CO, USA

[3]School of Geosciences, University of South Florida, Tampa, FL, USA

[4]Barcelona Supercomputing Center, Barcelona, Spain

[5]WeatherTiger, Tallahassee, FL, USA

[6]North Carolina State University (NCSU), Cooperative Institute for Satellite Earth System Studies (CISESS), Asheville, NC, USA

Corresponding author: Kimberly M. Wood (kimberly.wood@msstate.edu)

Key Points:

- Most 2019 Atlantic tropical cyclone activity occurred during a 6-week period of conducive environmental conditions.
- The subtropical Atlantic was more favorable than normal for tropical cyclones.
- The strongly positive Indian Ocean Dipole likely contributed to below-normal Atlantic tropical cyclone activity in October.

This article has been accepted for publication and undergone full peer review but has not been through the copyediting, typesetting, pagination and proofreading process which may lead to differences between this version and the Version of Record. Please cite this article as doi: 10.1029/2020GL087781

Abstract

The 2019 Atlantic hurricane season exhibited above-average Accumulated Cyclone Energy—60% of which was produced by Hurricanes Dorian and Lorenzo. Most tropical cyclone (TC) activity was concentrated in a ~6-week period from late August to early October. During the early part of the season, relatively TC-unfavorable conditions persisted in the main development region (MDR). The MDR environment became largely favorable in September followed by an abrupt shift back to less conducive conditions in October coincident with a strongly positive Indian Ocean Dipole (IOD). The IOD produced an El Niño-like teleconnection pattern observed through 200-hPa velocity potential anomalies. In the subtropical Atlantic, above-average sea surface temperatures persisted for much of the season, which may have contributed to increased activity at higher latitudes. Given the neutral El Niño-Southern Oscillation conditions during the 2019 hurricane season, our study highlights the need for further analysis of IOD impacts on Atlantic TC activity.

Plain Language Summary

In 2019, the Atlantic produced above-average activity according to Accumulated Cyclone Energy (ACE), an index that captures storm intensity and longevity. The two strongest hurricanes, Dorian and Lorenzo, contributed 60% of the season's total ACE. Most storms occurred in an active 6-week period from late August to early October when the environment became more favorable for hurricanes. But after that, conditions became less favorable when the western Indian Ocean became much warmer than normal and the eastern Indian Ocean became much colder than normal, an oceanic phenomenon referred to as a positive Indian Ocean Dipole. This strong positive Indian Ocean Dipole event produced sinking air across much of the tropics, including the Atlantic, a pattern that is El Niño-like. Since knowledge of El Niño helps us predict Atlantic seasonal hurricane activity, it is possible that understanding more about the Indian Ocean Dipole's impacts on Atlantic hurricane activity will help us improve seasonal hurricane forecasts.

1 Introduction

The 2019 Atlantic hurricane season reached above-average activity per the National Oceanic and Atmospheric Administration (NOAA) definition (https://www.cpc.ncep.noaa.gov/products/outlooks/archives/hurricane2017/August/NorATL_Background.shtml), with 18 named storms (1-minute maximum sustained winds ≥ 34 kt or 15.4 m s^{-1}), 6 hurricanes (winds ≥ 64 kt), 3 major hurricanes (Category 3+ on the Saffir-Simpson Hurricane Wind Scale; winds ≥ 96 kt), and an ACE index of 132.2×10^4 kt^2 (Accumulated Cyclone Energy; Bell et al., 2000). The 1981-2010 average—the current 30-year averaging period used by NOAA for climate analysis—is 12.1 named storms, 6.4 hurricanes, 2.7 major hurricanes, and an ACE index of 105.6×10^4 kt^2. The 2019 Atlantic hurricane season generated ACE that was 125% of the 1981-2010 average. Over 60% of the 2019 ACE was generated by two storms: Dorian and Lorenzo. Hurricane Dorian produced 48.9×10^4 kt^2 alone (37% of the season's ACE), ranking 9th for most ACE generated by an individual Atlantic tropical cyclone (TC) during the satellite era (1966-2019).

The strongest 2019 Atlantic TC was also the most damaging. Hurricane Dorian made landfall on the island of Great Abaco in the Bahamas at peak intensity (160 kt), making it the strongest Atlantic hurricane in the satellite era (since 1966; Vecchi & Knutson, 2011) outside of the tropics (>23.5°N) and the strongest hurricane on record to hit the Bahamas (Avila et al., 2020). Dorian's slow forward speed and proximity to warm waters resulted in its core devastating the northwestern Bahamas for at least 48 hours. Though Dorian weakened from a Category 5 to a Category 2 hurricane during this period, the Bahamian death toll estimates range from 74 to more than 200 with damages estimated at $3.4 billion USD (Avila et al., 2020). A few weeks later, Hurricane Lorenzo reached 140 kt and became the first Atlantic Category 5 hurricane on record east of 50°W (Zelinsky, 2019). At least 19 people lost their lives due to marine hazards from Lorenzo, with eleven of these fatalities associated with the sinking of the ship *Bourbon Rhode*.

During the 2019 Atlantic hurricane season, El Niño-Southern Oscillation (ENSO) entered a neutral state after a weak El Niño event that spanned January – June 2019 per NOAA's ENSO diagnostics discussions (https://www.cpc.ncep.noaa.gov/products/expert_assessment/ENSO_DD_archive.php). On the other hand, the Indian Ocean Dipole (IOD; Saji & Yamagata, 2003) reached unprecedented positive values, indicating that the western Indian Ocean was much warmer than normal concurrently with the eastern Indian Ocean being much cooler than normal. Though ENSO has been independently linked to Atlantic TC activity (e.g., Gray, 1984; and many others) and to the IOD (Wang et al., 2019), only one study has investigated the relationship between concurrent IOD conditions and Atlantic TC activity. In the 2011 State of the Climate report, Bell et al. (2012) examined eight significant positive IOD events since 1979, one of which occurred during a neutral ENSO phase, and found below-normal Atlantic activity for seven of the eight years (the eighth was a La Niña year). They speculated that the positive IOD phase in 2011 may have contributed to lower TC activity than anticipated by the NOAA seasonal outlook.

In this study, we examine seasonal variability of atmospheric fields and sea surface temperature (SST) and assess their impact on 2019 Atlantic TC activity. We also build from Bell et al. (2012) by exploring the role of the record-breaking positive IOD event on the 2019 Atlantic hurricane season to motivate future work on the IOD's relationship with Atlantic TC activity.

2 Data and Methods

Metrics of Atlantic TC activity considered in this manuscript include named storms, hurricanes, major hurricanes, and ACE calculated from the second-generation Hurricane Best Track dataset (HURDAT2; Landsea & Franklin, 2013) updated for 2019 TCs on 28 April 2020.

The 0.25° Fifth-generation European Centre for Medium-range Weather Forecasts (ECMWF) Reanalysis (ERA5) is available from 1979 to present (Hersbach et al., 2020). We obtain monthly-averaged ERA5 fields from ECMWF's Copernicus Climate Data Store (CDS; https://cds.climate.copernicus.eu/). Variables we compute from ERA5 data include vertical wind shear—the vector wind difference between 200 and 850 hPa—and 200-hPa velocity potential. We evaluate velocity potential because the irrotational (divergent) wind is the gradient of velocity potential. Thus, below-average velocity potential (i.e., negative velocity potential anomalies) corresponds to divergence and can indicate upper-level support for rising motion. We calculate velocity potential from ERA5 zonal and meridional wind using the Python package *windspharm* (Dawson, 2016). Since ERA5 data are currently limited to 1979-present, we also obtain fields from the National Centers for Environmental Prediction (NCEP)/National Center for Atmospheric Research (NCAR) Reanalysis (Kalnay et al., 1996) to extend our analysis farther back in time.

To evaluate behavior of the Madden-Julian oscillation (MJO), we rely on the Wheeler-Hendon index (Wheeler & Hendon, 2004) obtained from the Australian Bureau of Meteorology (http://www.bom.gov.au/climate/mjo/graphics/rmm.74toRealtime.txt). This index removes the 120-day running average from upper- and lower-level zonal wind as well as outgoing longwave radiation to better highlight the MJO's subseasonal signal and reduce the longer-term signal from ENSO.

We explore SST with monthly, 1° fields from the Centennial in-situ Observation-Based Estimates (COBE) dataset maintained by the Japan Meteorological Agency (Ishii et al., 2005) which we download from https://ds.data.jma.go.jp/tcc/tcc/products/elnino/cobesst/cobe-sst.html. COBE SST data begin in 1891 and enable longer-term exploration of the IOD. The IOD is defined as the SST anomaly difference between the western and eastern Indian Ocean. Thus, we calculate the IOD index by subtracting the SST anomaly over the eastern Indian Ocean (10°S-0°, 90°-110°E) from the SST anomaly over the western Indian Ocean (10°S-10°N, 50°-70°E). A positive IOD implies the western anomaly is greater than the eastern anomaly, and a negative IOD implies the western anomaly is less than the eastern anomaly. We compute these SST anomalies relative to the 1981-2010 base period.

To assess ENSO, we rely on NOAA's Oceanic Niño Index (ONI). The ONI covers 1950-present using 3-month-averaged SST anomalies in the region 5°S-5°N, 170-120°W from version 5 of the Extended Reconstructed Sea Surface Temperature dataset (Huang et al., 2017). These SST anomalies are calculated from centered 30-year base periods updated every 5 years (https://origin.cpc.ncep.noaa.gov/products/analysis_monitoring/ensostuff/ONI_change.shtml). El Niño events are declared when the ONI reaches at least 0.5°C for five consecutive months and La Niña events when the ONI is at or below -0.5°C for five consecutive months. Atmospheric anomalies must also be consistent with El Niño or La Niña for NOAA to declare an event.

To provide context for 2019 conditions, we compute z-scores for the Atlantic main development region (MDR; 10-20°N, 80-20°W; Vecchi & Knutson, 2011) and the subtropical Atlantic (20-35°N, 75-30°W). A z-score, also known as a standardized anomaly, enables intercomparison of normally distributed variables that have different values and value ranges. For normally distributed data, 95% of the observations should have z-scores between -1.96 and 1.96, thus z-scores beyond these values would be considered statistically significant at the 5% level. In this study, each z-score is calculated by subtracting the 1981-2010 average from the 2019 value and then dividing that difference by the 1981-2010 standard deviation for available fields such as SST and relative humidity as well as derived fields such as velocity potential and 200-850–hPa vertical wind shear.

Finally, we evaluate the ACE-IOD relationship via partial rank correlation (http://vassarstats.net/textbook/ch3a.html) to remove the effect of ENSO:

$$r_{xy\cdot z} = \frac{r_{xy} - r_{xz}r_{yz}}{\sqrt{(1 - {r_{xz}}^2)(1 - {r_{yz}}^2)}}$$

where *r* is the Spearman rank correlation between two fields and *x* represents ACE, *y* the IOD index, and *z* the ONI.

3 Overview of the 2019 Atlantic hurricane season

Atlantic TC activity, as measured by ACE, was at or below normal until September (Fig. 1a). No named storms formed from 12 July – 20 August, the first time this 39-day period had 0 named storm formations since 1982. An active period immediately followed: 10 named storms developed between 21 August – 23 September, tying 1949 and 2010 for the most named storms on record to form during this 33-day period. September was dominated by the four TCs that contributed the most ACE (Dorian, Humberto, Jerry, and Lorenzo; Fig. 1b), with Dorian and Lorenzo contributing ~60% of the season's ACE.

Not only was Dorian the strongest recorded TC to make landfall in the Bahamas, but the duration of catastrophic wind and surge conditions on Great Abaco and Grand Bahama Islands was exceptional. The 11.4 total units of ACE expended by Dorian in a 1°-by-1° grid box centered on Grand Bahama are the maximum local, single-storm ACE anywhere in the Atlantic basin during the satellite era.

Multiple TCs occurred in October, but most were weak and/or short-lived, resulting in below-average October ACE. Figure 1b highlights the imbalanced individual TC contributions to total ACE: 14 of the 18 named storms *combined* produced only 21% of the season's ACE. But weaker TCs can still produce widespread impacts: Imelda had an intensity of only 40 kt when it made landfall but then tracked extremely slowly across Texas, where flooding from heavy rainfall resulted in 5 deaths and economic damages of $5 billion USD (Latto & Berg, 2020).

Of 2019's 18 named storms, 6 became hurricanes. Only four other seasons since 1966 had 33% or fewer named storms become hurricanes: 2013 (14%) and 1982, 2002, and 2009 (33%). We note that technological advances, such as polar-orbiting scatterometers, likely enabled improved detection of TCs lasting 2 days or fewer since 2000 (Landsea et al., 2010; Villarini et al., 2011).

4 Environmental factors affecting 2019 TC activity

Sea surface temperatures serve as one of the most important factors driving Atlantic TC activity on seasonal timescales (e.g., Saunders et al., 2017, and references therein), with above-average SSTs generally favoring more active Atlantic hurricane seasons. June 2019 SSTs in the MDR were near the 1981-2010 average, but these SSTs climbed to 0.5-1.0°C above normal for the peak Atlantic hurricane season months of August-October (Fig. S1). Above-average SSTs likely helped fuel the highly active September, but other dynamic and thermodynamic conditions discussed later in this section may have inhibited TC activity in both August and October.

Vertical wind shear is generally detrimental to TC development and intensification (e.g., Kaplan & DeMaria, 2003). In the Atlantic, shear tends to be favorable from late June until mid-October (e.g., De Maria et al., 2001). For June 2019, climatologically unfavorable shear was stronger than normal and may have contributed to the lack of TCs during that month (Fig. 2a). Though shear weakened relative to climatology in July, only Hurricane Barry developed over the Gulf of Mexico from a non-tropical system (Cangialosi et al., 2019). Note that other factors beyond shear contribute to climatologically low July Atlantic TC activity (Fig. 1a), such as a stable atmosphere (e.g., DeMaria et al., 2001).

August 2019 exhibited below-average Atlantic TC activity (Fig. 1a). Despite relatively favorable shear conditions, only Tropical Storm Chantal formed in the subtropics prior to Dorian's development and subsequent intensification late in the month (Fig. 2c). Dry air in the mid-levels likely acted as a primary suppressive factor during August. Consistent with climatology, September was the most active month in 2019. September exhibited below-average shear across most of the tropical Atlantic and the Gulf of Mexico, with much of the tropical Atlantic also characterized by above-average moisture (Fig. 2d). However, Atlantic MDR moisture plummeted in October, when most activity was confined to the Gulf of Mexico and higher latitudes where both greater moisture and lower shear dominated (Fig. 2e). October featured five named storms, but due to relatively TC-unfavorable conditions, just one (Pablo) reached hurricane strength, sustaining that intensity for only 12 h (Beven, 2020). The lone November storm, Sebastien, traversed a higher moisture and lower shear region in the central Atlantic (Fig. 2f).

Given 2019's relatively infrequent activity at low latitudes and the number of TCs poleward of 20°N (Fig. 2), we next evaluate the conditions in these two regions within the context of 1981-2010 averages (Fig. 3). In the MDR, higher shear, positive velocity potential anomalies, and drier air prevailed during June when no TC activity occurred (Fig. 3a). July became marginally more favorable, but August anomalies resembled June anomalies, dominated by less conducive conditions, particularly in the eastern part of the MDR (Fig. 2c). Conditions became more conducive for TCs in September when shear decreased, moisture and SSTs increased, and support for rising motion increased. However, MDR conditions nearly flipped in October, when only SST remained conducive and the mid-level relative humidity z-score broached -1.96, indicating statistically significant dry anomalies (Fig. 3a).

In contrast to the MDR, 2019 subtropical Atlantic conditions were primarily more conducive than normal (Fig. 3b). Area-averaged SST remained above normal throughout the season and exceeded the significance threshold from July-September. Vertical wind shear was particularly low in August relative to climatology, and September was marked by rising motion and increased moisture in addition to more conducive SST.

The shift of MDR conditions from favorable in September to unfavorable in October requires further assessment given the prevailing ENSO-neutral conditions during both months. One might suspect the MJO to be responsible for this relatively abrupt transition, as the oscillation is known to impact TC formation (Klotzbach & Oliver, 2015). However, according to the Wheeler-Hendon index, the MJO was in phases 1 and 2 for 18 of the first 23 days in October (Fig. S2), phases typically associated with active periods for Atlantic hurricane activity (Klotzbach & Oliver, 2015). Consequently, we now look elsewhere for physical mechanisms that may have inhibited October activity.

In October 2019, the IOD reached a record positive value of 2.22, exceeding the previous record of 1.82 set in October 1994. The strongly positive IOD likely contributed to a global pattern of 200-hPa velocity potential anomalies that supported enhanced rising motion over Africa and the western Indian Ocean with enhanced sinking across much of the rest of the tropics (Fig. 4a). As shown earlier (Fig. 3a), these positive velocity potential anomalies extended into the MDR. The October 2019 velocity potential anomaly pattern is a stronger version of the pattern associated with a positive IOD over the 60-year period from 1960 to 2019 (Fig. 4b), which is itself a weaker version of what tends to occur during El Niño events (Fig. 4c). October's strongly positive IOD value is unprecedented in the satellite era and unusual for an ENSO-neutral event (Fig. 5a). Given that the record positive IOD occurred in an October with ENSO-neutral conditions, it likely helped to concentrate upward motion over Africa and the western Indian Ocean while simultaneously suppressing upward motion over the tropical Atlantic.

Positive IOD events often occur at the same time as El Niño events as evidenced by a correlation coefficient of 0.51 between October IOD and ONI (Fig. 5a). This relationship may be a consequence of Pacific warming leading to enhanced anticyclonic vorticity over the western Indian Ocean that counteracts the Indian monsoon flow, reducing surface wind stress and thus increasing western Indian Ocean SST (Fan et al., 2017). The relationship between the IOD and ACE reached its strongest magnitude ($r_{rank} \approx$ -0.70) during the largely negative phase of the Atlantic Multi-decadal Oscillation (AMO) from the late 1960s through the late 1990s (Goldenberg et al., 2001), a relationship that has weakened since then (Fig. 5b). Caron et al. (2015) noted similar changes in drivers of Atlantic TC activity caused by AMO phase changes. Our preliminary analysis indicates that the inverse relationship between the IOD and vertical wind shear was stronger during the 1970-1994 negative AMO than during the 1995-2019 positive AMO (not shown). We intend to investigate this relationship in future work. Regardless of AMO phase, the IOD shows a strong correlation with positive velocity potential anomalies—and thus suppressed upward motion—during October compared with earlier in the season (Fig. 5c).

5 Conclusions

This study investigates the 2019 Atlantic hurricane season, a season dominated by ENSO-neutral conditions. The MDR environment (10-20°N, 80-20°W) was relatively unfavorable during August, contributing to a less active month in terms of ACE (66% of normal). Conditions became much more conducive in September when the Atlantic generated 182% of normal ACE for the month, part of a 6-week period of concentrated TC activity. Though five named storms developed during October, most of these storms were weak and short-lived, producing ACE that was 87% of normal. In general, unfavorable mid-level moisture and less support for rising motion may have suppressed TC activity during August and October. Higher latitudes in the Atlantic were relatively favorable for TCs compared to normal, particularly SST.

The Indian Ocean Dipole's unprecedented positive value likely contributed to an El Niño-like pattern of rising and sinking motion across the tropics—an effect more apparent due to ENSO-neutral conditions—and thus helped suppress October TC activity in the Atlantic despite a more TC-favorable MJO phase. No TCs occurred within the MDR in October, an outcome that supports previous findings of generally suppressed Atlantic TC activity during positive IOD events (Bell et al., 2012). Seasonal hurricane forecasts are challenging during neutral ENSO events because TC activity under such conditions has historically varied from extremely quiet to extremely active. Further assessment of the relationship between the IOD and TC activity could aid seasonal forecasts in future years.

Acknowledgments

All data examined in this study are available from the UCAR, ECMWF, NCEP, and JMA websites cited in the text. Many figures were produced using Matplotlib (https://matplotlib.org/) and Cartopy (https://scitools.org.uk/cartopy/docs/latest/). K. Wood was supported by the Office of Research and Economic Development and the Department of Geosciences at Mississippi State University. P. Klotzbach acknowledges a grant from the G. Unger Vetlesen Foundation. C. Schreck was supported by NOAA through the Cooperative Institute for Satellite Earth System Studies under Cooperative Agreement NA19NES4320002. The authors thank Dr. Chris Landsea and an anonymous reviewer for their helpful feedback, especially during the COVID-19 pandemic.

References

Avila, L. A., Stewart, S. R., Berg, R., & Hagen, A. B. (2020). Hurricane Dorian. National Hurricane Center Tropical Cyclone Report, NHC, 74 pp. https://www.nhc.noaa.gov/data/tcr/AL052019_Dorian.pdf

Bell, G. D., Halpert, M. S., Schnell, R. C., Higgins, R. W., Lawrimore, J., Kousky, V. E., *et al.* (2000). Climate assessment for 1999. *Bulletin of the American Meteorological Society*, **81**, S1–S50. https://doi.org/10.1175/1520-0477(2000)81[s1:CAF]2.0.CO;2

Bell, G. D., Blake, E. S., Landsea, C. W., Kimberlain, T. B., Goldenberg, S. B., Schemm, J., & Pasch, R. J. (2012). Tropical Cyclones - Atlantic Basin, State of the Climate in 2011. *Bulletin of the American Meteorological Society*, **93**, S99-S105. https://doi.org/10.1175/2012BAMSStateoftheClimate.1

Beven, J. L. (2020). Hurricane Pablo. National Hurricane Center Tropical Cyclone Report, NHC, 12 pp. https://www.nhc.noaa.gov/data/tcr/AL182019_Pablo.pdf

Cangialosi, J. P., Hagen, A. B., & Berg, R. (2019). Hurricane Barry. National Hurricane Center Tropical Cyclone Report, NHC, 31 pp. https://www.nhc.noaa.gov/data/tcr/AL022019_Barry.pdf

Caron, L.-P., Boudreault, M., & Bruyere, C. L. (2015). Changes in large-scale controls of Atlantic tropical cyclone activity with the phases of the Atlantic multidecadal oscillation. *Climate Dynamics,* **44,** 1801-1821. https://doi.org/10.1007/s00382-014-2186-5

Dawson, A. (2016). Windspharm: A High-Level Library for Global Wind Field Computations Using Spherical Harmonics. *Journal of Open Research Software,* **4**, p.e31. https://doi.org/10.5334/jors.129

Goldenberg, S. B., Landsea, C. W., Mestas-Nunez, A. M., & Gray, W. M. (2001). The recent increase in Atlantic hurricane activity: Causes and implications. *Science*, **293**, 474-479. https://doi.org/10.1126/science.1060040

Gray, W. M. (1984). Atlantic seasonal hurricane frequency. Part I: El Niño and 30 mb quasi-biennial oscillation influences. *Monthly Weather Review*, **112**, 1649–1668. https://doi.org/10.1175/1520-0493(1984)112<1649:ASHFPI>2.0.CO;2

Hersbach, H., Bell, W., Berrisford, P., Horányi, A., Muñoz-Sabater, J., Nicolas, J., Radu, R., *et al* (2019). Global reanalysis: goodbye ERA-Interim, hello ERA5. *ECMWF Newsletter*, **159**, 17-24. https://doi.org/10.21957/vf291hehd7

Huang, B., Thorne, P. W., Banzon, V. F., Boyer, T., Chepurin, G., Lawrimore, J. H. (2017). Extended reconstructed sea surface temperature version 5 (ERSSTv5): Upgrades, validations and intercomparisons. *Journal of Climate*, **30,** 8179-8205. https://doi.org/10.1175/JCLI-D-16-0836.1

Ishii, M., Shouji, A., Sugimoto, S., & Matsumoto, T. (2005). Objective Analyses of Sea-Surface Temperature and Marine Meteorological Variables for the 20th Century using ICOADS and the Kobe Collection. *International Journal of Climatology*, **25**, 865-879. https://doi.org/10.1002/joc.1169

Kalnay, E., Kanamitsu, M., Kistler, R., Collins, W., Deaven, D., Gandin, L., *et al.* (1996). The NCEP/NCAR 40-Year Reanalysis Project. *Bulletin of the American Meteorological Society*, **77**, 437–472. https://doi.org/10.1175/1520-0477(1996)077<0437:TNYRP>2.0.CO;2

Kaplan, J., & DeMaria, M. (2003). Large-scale characteristics of rapidly intensifying tropical cyclones in the North Atlantic basin. *Weather and Forecasting*, **18**, 1093–1108. https://doi.org/10.1175/1520-0434(2003)018<1093:LCORIT>2.0.CO;2

Klotzbach, P. J., & Oliver, E. C. (2015). Modulation of Atlantic Basin Tropical Cyclone Activity by the Madden–Julian Oscillation (MJO) from 1905 to 2011. *Journal of Climate*, **28**, 204–217. https://doi.org/10.1175/JCLI-D-14-00509.1

Landsea, C.W., Vecchi, G.A., Bengtsson, L., & Knutson, T. R. (2010). Impact of Duration Thresholds on Atlantic Tropical Cyclone Counts. *Journal of Climate*, **23**, 2508–2519. https://doi.org/10.1175/2009JCLI3034.1

Landsea, C. W., & Franklin, J. L. (2013). Atlantic hurricane database uncertainty and presentation of a new database format. *Monthly Weather Review*, **141**, 3576–3592. https://doi.org/10.1175/MWR-D-12-00254.1

Latto, A., & Berg, R. (2020). Tropical Storm Imelda. National Hurricane Center Tropical Cyclone Report, NHC, 28 pp. https://www.nhc.noaa.gov/data/tcr/AL112019_Imelda.pdf

Saji, N. H., & Yamagata, T. (2003). Possible impacts of Indian Ocean dipole mode events on global climate. *Climate Research*, **25**, 151–169. https://doi.org/10.3354/cr025151

Saunders, M. A., Klotzbach, P. J., & Lea, A. S. R. (2017). Replicating annual North Atlantic hurricane activity 1878-2012 from environmental variables. *Journal of Geophysical Research Atmospheres,* **122,** 6284-6297, https://doi.org/10.1002/2017JD026492

Vecchi, G.A., Knutson, T.R. (2011). Estimating annual numbers of Atlantic hurricanes missing from the HURDAT database (1878-1965) using ship track density. *Journal of Climate,* **24,** 1736-1746. https://doi.org/10.1175/2010JCLI3810.1

Villarini, G., Vecchi, G.A., Knutson, T.R., & Smith, J.A. (2011). Is the Recorded Increase in Short Duration North Atlantic Tropical Storms Spurious? *Journal of Geophysical Research*, **116**, D10114. https://doi.org/10.1029/2010JD015493

Wang, H., Kumar, A., Murtugudde, R., Narapusetty, B., & Seip, K. L. (2019). Covariations between the Indian Ocean dipole and ENSO: a modeling study. *Climate Dynamics,* **53,** 5743–5761. https://doi.org/10.1007/s00382-019-04895-x

Wheeler, M.C., & Hendon, H.H. (2004). An all-season real-time multivariate MJO index: Development of an index for monitoring and prediction. *Monthly Weather Review*, **132**, 1917–1932. https://doi.org/10.1175/1520-0493(2004)132<1917:AARMMI>2.0.CO;2

Zelinsky, D. A. (2019). Hurricane Lorenzo. National Hurricane Center Tropical Cyclone Report, NHC, 22 pp. https://www.nhc.noaa.gov/data/tcr/AL132019_Lorenzo.pdf

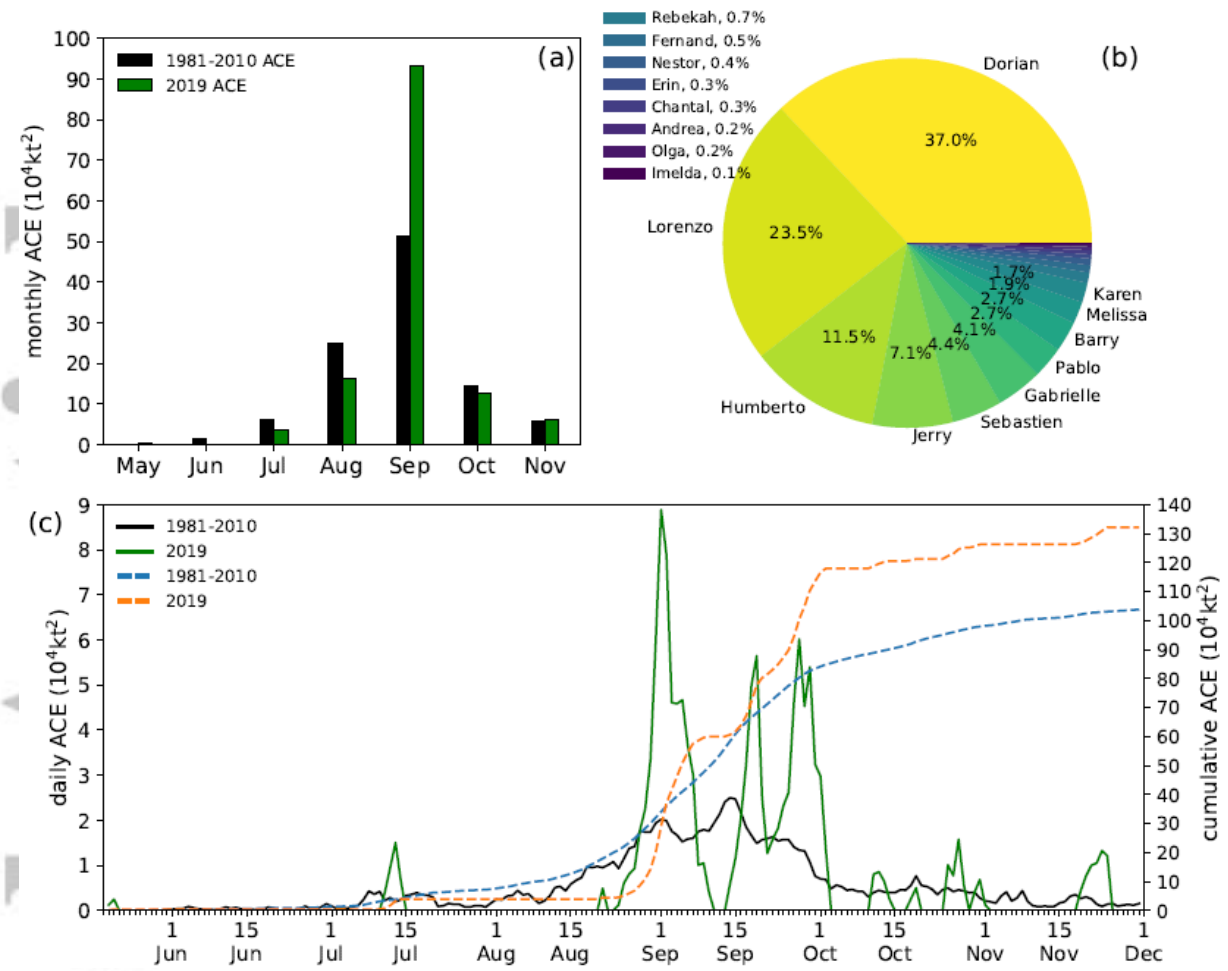

Figure 1. (a) Monthly Accumulated Cyclone Energy (ACE; 10^4 kt^2) for 1981-2010 (black) and 2019 (green). May is included because Subtropical Storm Andrea developed prior to the official start of the hurricane season on 1 June. (b) Individual TC contributions to ACE ordered counterclockwise from greatest to least. Two TCs—Dorian and Lorenzo—produced more than 60% of the season's total ACE, and seven TCs each contributed less than 1%. (c) Daily ACE and accumulated ACE during the 2019 season and averaged for 1981-2010, highlighting the increased TC activity from late August through early October 2019.

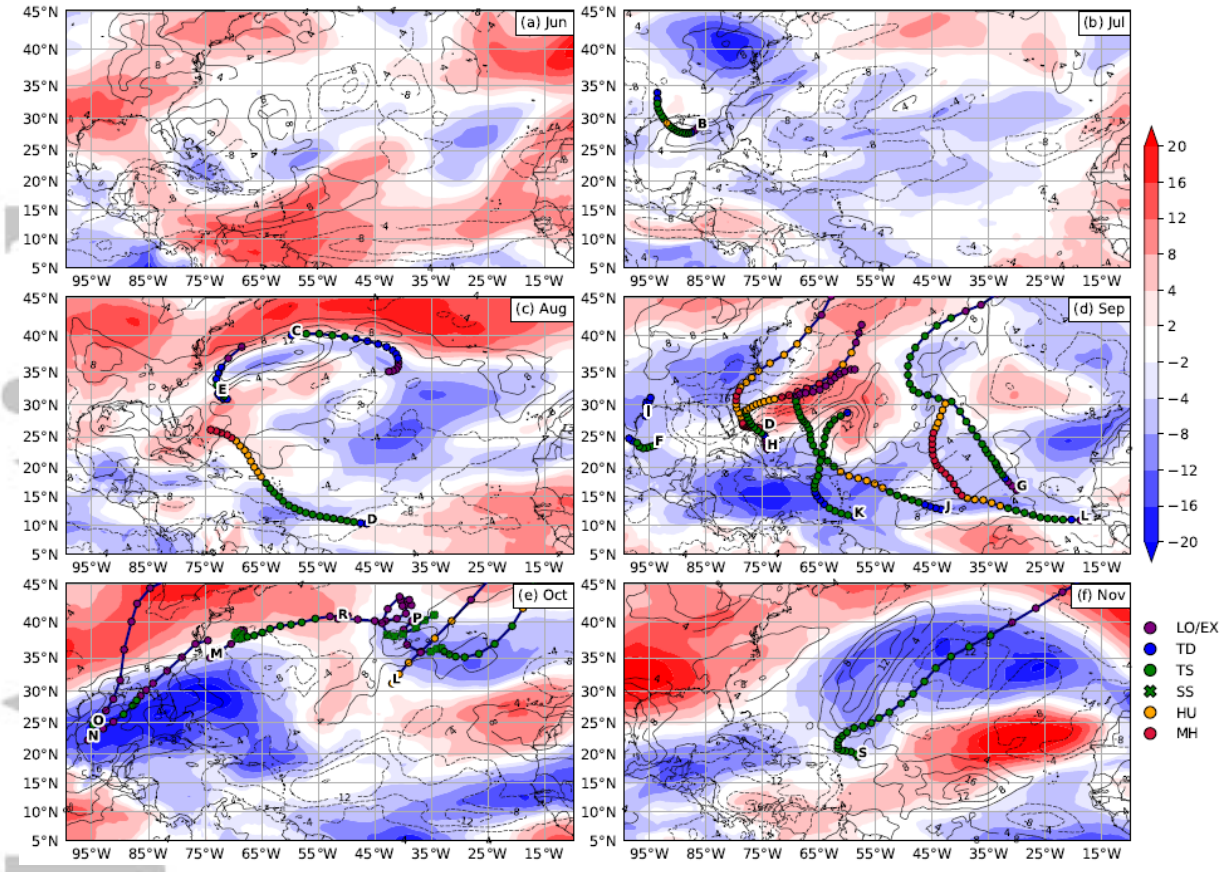

Figure 2. 200-850–hPa vertical wind shear anomalies (kt; shaded) and 500-700–hPa relative humidity anomalies (%; contours) relative to 1981-2010 during (a) June, (b) July, (c) August, (d) September, (e) October, and (f) November 2019. Lines represent the portion of TC tracks with maximum lifetime intensities of at least 34 kt that occurred in the given month; symbols represent storm status every 6 h.

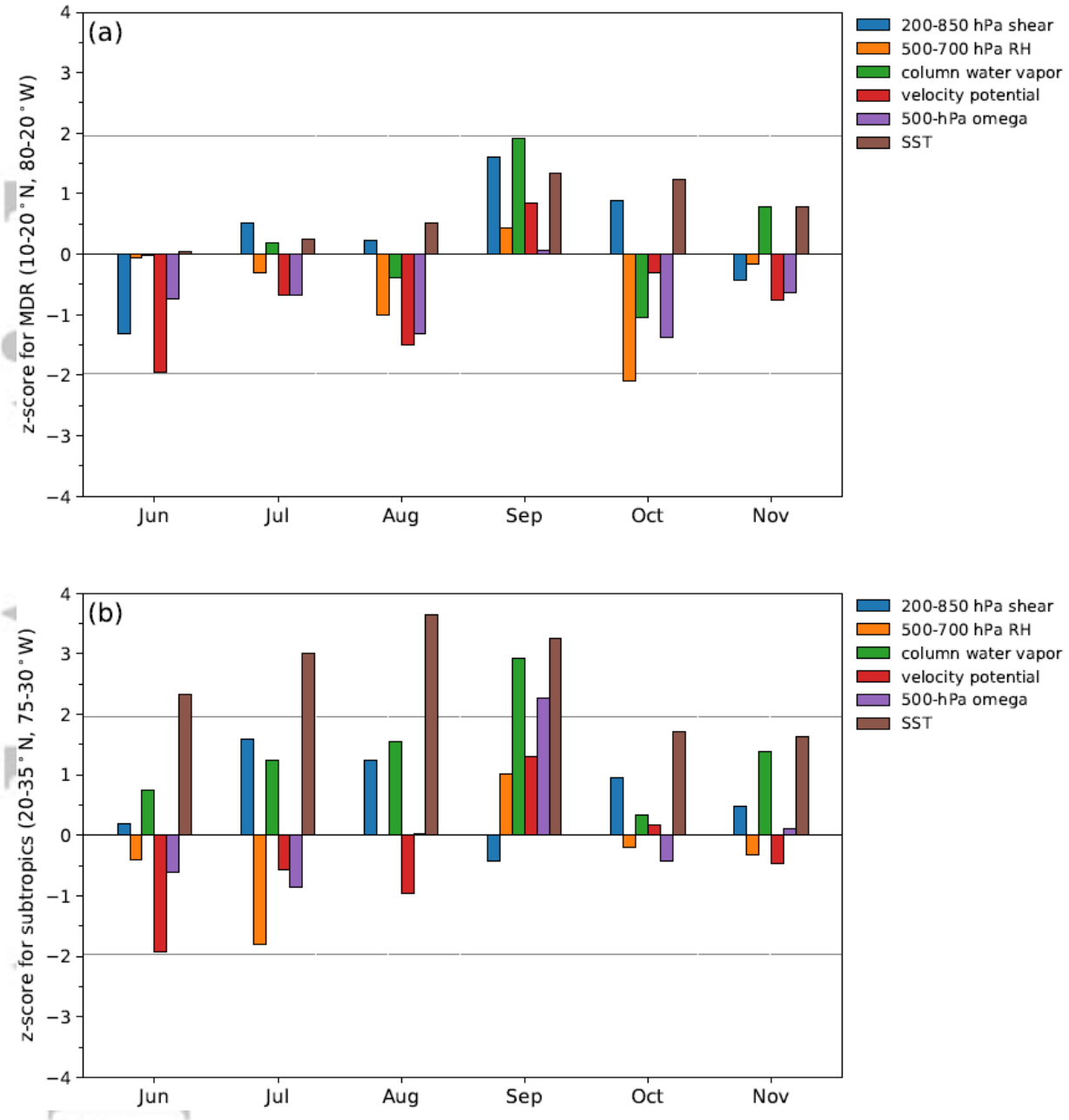

Figure 3. Z-scores for monthly ERA5 200-850–hPa vertical wind shear, 500-700–hPa relative humidity (RH), total column water vapor, 200-hPa velocity potential anomalies, 500-hPa vertical velocity (omega), and COBE SST calculated for (a) the Atlantic MDR (10-20°N, 80-20°W) and (b) the subtropical Atlantic (20-35°N, 75-30°W). All z-scores are computed relative to 1981-2010. For shear, velocity potential, and omega, the signs have been reversed such that, for all included fields, positive z-scores indicate more favorable conditions for TCs, and negative z-scores indicate less favorable.

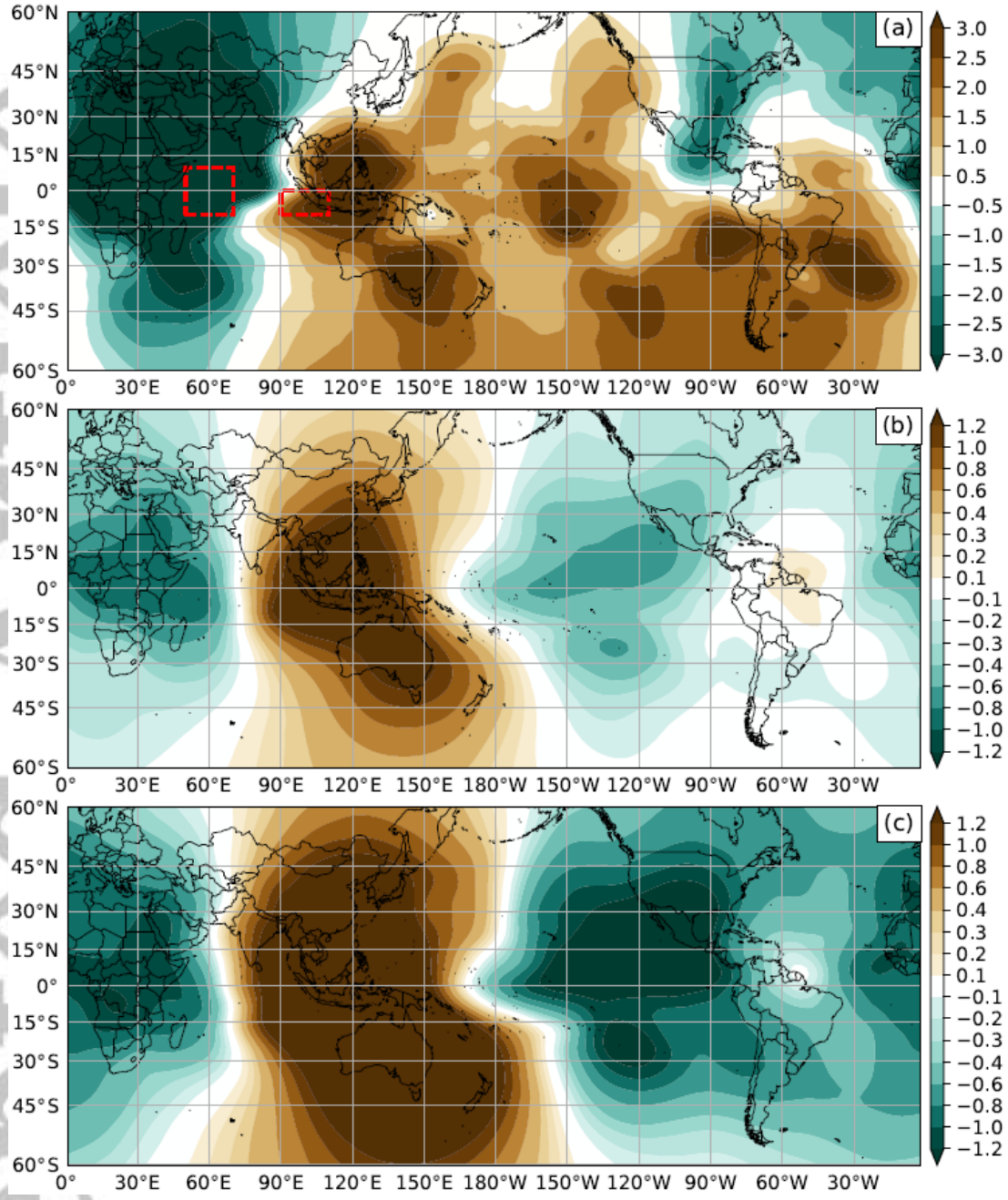

Figure 4. 200-hPa velocity potential anomalies (10^6 m^2 s^{-1}) relative to 1981-2010. (a) October 2019 from ERA5. Dashed red boxes indicate the western and eastern regions used to calculate the IOD index. (b) October 1960-2019 NCEP/NCAR Reanalysis anomalies regressed onto the October 1960-2019 COBE IOD index. (c) October 1960-2019 NCEP/NCAR Reanalysis anomalies regressed onto the October 1960-2019 NINO3.4 anomalies used to calculate the ONI.

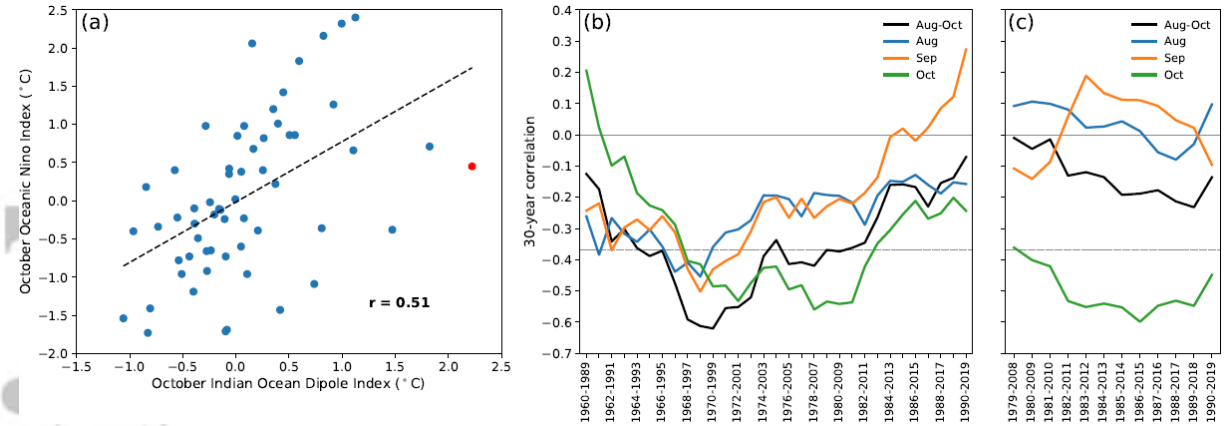

Figure 5. (a) October IOD index versus October ONI values during 1960-2019 (red dot indicates October 2019). The dashed black line shows the linear regression between the two indices (r = 0.51). (b) Partial rank correlations between Atlantic ACE and the IOD index with the ONI removed for running 30-year periods during 1960-2019 for August-October (black), August (blue), September (orange), and October (green). The horizontal dashed line represents 5% statistical significance. (c) As in (b) but computed between ERA5 200-hPa velocity potential anomalies in the MDR and the IOD index during 1979-2019.